Available online at www.sciencedirect.com
ScienceDirect
Journal of Magnesium and Alloys xxx (xxxx) xxx
www.elsevier.com/locate/jma

Full Length Article

Inhibiting creep in fine-grained Mg–Al alloys through grain boundary stabilization

Lingbao Ren[a,*], Yurong Zhao[a], Jinjin Li[a], Fei Liu[a], Boyu Liu[a], Ge Wu[a], Carl J. Boehlert[b], Zhiwei Shan[a,*]

[a] *Center for Advancing Materials Performance from the Nanoscale, State Key Laboratory for Mechanical Behavior of Materials, Xi'an Jiaotong University, Xi'an 710049, PR China*

[b] *Department of Chemical Engineering and Materials Science, Michigan State University, East Lansing, MI 48824, United States*

Received 9 March 2024; received in revised form 19 April 2024; accepted 29 April 2024
Available online xxx

Abstract

The limited creep resistance of wrought Mg–Al alloys restricts their lightweight applications at intermediate temperatures due to the softening effect of discontinuous precipitation (DP) on the dislocation-controlled creep. Here, we developed a creep-resistant wrought Mg–Al alloy through microalloying of Y and Ca. The resulting alloy exhibited an order of magnitude enhancement in the creep resistance at 125 °C/50–100 MPa. In contrast to the grain boundary instabilities by DP in the previously reported wrought Mg–Al alloys, we show that the addition of 0.21Y+0.15Ca wt% produces a (Zn+Ca) co-segregation at the grain boundaries as a result of their segregation energy and the activation energy of grain boundary migration, thereby stabilizing the grain boundaries. The (Zn+Ca) co-segregation inhibits the dynamic DP and promotes the formation of intragranular Al-enriched clusters, which favorthe formation of Al_2Y, $Mg_{17}Al_{12}$ nano precipitates, thereby impeding intragranular dislocation motion during creep. Furthermore, the addition of 0.21Y+0.15Ca wt% facilitates the formation of a fine and uniform recrystallization structure in the microalloyed alloys compared to AZ80 due to the high activation energy of mobility for the (Zn+Ca) segregated grain boundary. Therefore, the microalloyed alloys exhibit good tensile properties with 380 MPa tensile strength and 18 % elongation. Our constitutive analysis revealed that the (Y+Ca) microalloying decreased the creep stress exponent by 29 % and increased the creep resistance in the medium to high-stress range. Microalloying provides a promising way to develop low-cost creep-resistant wrought Mg–Al alloys.

Keywords: Creep; Wrought Mg alloys; Discontinuous precipitation; Microalloying; Segregation.

1. Introduction

Mg is one of the lightest structural metals. The medium-temperature creep resistance of Mg–Al wrought alloys is limited, which presents challenges to meeting the demand service requirements of lightweight power components used in the automotive industry [1,2]. For instance, Mg–Al alloys should withstand stress levels of up to 100 MPa in transmission housings exposed to temperatures of around 100 °C [3]. These Mg–Al alloys should also be able to bear long-term loads without deformation or even cracking at higher temperatures, which is known as creep resistance [4]. Other applications, such as building framework (adiabatic temperature rise of concrete: ~100 °C) [5], battery compartments for automobiles (~90 °C) [6], etc., also require similar creep resistance. Therefore, the creep resistance of high-strength Mg alloys under medium temperature conditions needs further study.

The design of creep-resistant Mg alloys typically aims to reduce or eliminate crystal defects related to deformation creep [7,8], such as grain boundaries. A single crystal or a coarse crystal matrix can be chosen and further reinforced by a high-content rare-earth alloying strategy to prevent in-

* Corresponding authors.
E-mail addresses: renlingbao@xjtu.edu.cn (L. Ren), zwshan@mail.xjtu.edu.cn (Z. Shan).

https://doi.org/10.1016/j.jma.2024.04.033

tragranular creep dislocation movement [9,10]. Alternatively, a high thermal-stability second phase can be selected to prevent intragranular dislocation or grain boundary movement [11–13]. Thereby improving the intragranular structure's dynamic stability during the creep process. Habibi Eftekhar et al. [14] reported that modifying the eutectic phase, globalizing α-Mg dendrites, and fragmenting the distributed secondary phase improved the intermediate-temperature creep resistance of AXE622 (Mg–5.88Al–1.62Ca–0.83Ce–0.46La, wt%) due to semisolid processing. Chen et al. [15] reported that 1.2Y+1.0Ca (wt%) addition contributed to an order of magnitude enhancement in the creep resistance of as-cast AZ61 alloys at 150 °C/50 MPa, where the ε_{min} decreased from 1.1 × 10^{-7} s^{-1} to 4.6 × 10^{-9} s^{-1}. Rare-earth containing Mg alloys [9], with heat-stable secondary phases, are typically produced through casting, which results in relatively large grains, low yield strength and plasticity, and high cost, making it challenging to meet the demands of high load, high safety, and cost-effectiveness.

Generally, wrought Mg alloys can maintain their strength and plasticity at room temperature through fine-grain strengthening [16]. At medium and high temperatures, the movement of dislocations and the diffusion of grain boundaries is more active compared to room temperature [7], leading to grain boundary sliding, rotation, and coarsening. As a result, the stability of the grain structure could be compromised, leading to significant creep deformation at medium and high temperatures during extended periods of use. Therefore, the creep resistance of fine-grained, deformed Mg-based materials is significantly lower when compared to that of a coarse-grained material at medium and high temperatures [17]. Developing fine-grained Mg alloys with both high mechanical strength and medium-temperature creep resistance is imperative to ensure long-term safe operation at elevated temperatures.

It has been widely reported that dislocation climb is the primary creep rate controlling mechanism for wrought Mg–Al alloys under medium temperature and high loading conditions [18] (σ/G = 10^{-3}–10^{-2}, T/T_m=0.4–0.5). The supersaturated α-Mg solid solution in wrought Mg–Al alloys tends to precipitate at grain boundaries (GBs) at medium temperature [19,20]. On the one hand, GB precipitation converts a large number of intragranular Al solute atoms into lamellar precipitates with alternating growth of α-Mg and β-$Mg_{17}Al_{12}$ lamellge near the grain boundaries [21,22], thereby reducing the Al solute strengthening effect and the availability of intragranular precipitation strengthening, resulting in the weakening of the resistance to intragranular creep dislocation movement [23]. On the other hand, the lamellar discontinuous precipitation (DP) at grain boundaries is often accompanied by movement of the α-Mg matrix grain into the adjacent grain, resulting in grain coarsening. The lamellar DP structure behind moving grain boundaries also provides more interfaces for grain boundary sliding, which promotes grain boundary movement and sliding [22]. It is essential to suppress the DP-induced GB migration and regulate the intragranular precipitation to enhance the medium-temperature creep resistance of wrought Mg–Al alloys. This approach enables the simultaneous improvement of creep resistance at both grain boundaries and ingrain while maintaining the excellent mechanical properties of the fine-grained matrix.

Microalloying is an economical and effective metallurgical design method to regulate the properties of Mg alloys [9,24–26]. Some results [27–29] on the Mg–Al series alloys, AZ80 (Mg–8Al–0.5Zn (wt%)), confirm that a small amount (<0.5 wt%) of alloying elements and their combinations (such as (Y+ Ca), (Y+Nd), etc.) can both inhibit the recrystallization GB migration during hot extrusion processing and obtain higher mechanical strength and fracture elongation [29]. The addition of trace (<0.5 wt%) alloying elements (Y, Nd, Ca, etc.) can effectively reduce the proportion of DP at medium temperature, inhibit the α-matrix GB migration, and improve the stability of GB [27]. Thus, the selection of appropriate microalloying elements and their combinations can effectively enhance the stability of the GB structure of AZ80 at elevated temperatures. This inspired us to improve the stability of the GB structure during the medium-temperature creep process while maintaining the fine-grain structure of wrought AZ80 alloy by microalloying.

This study focused on the effect of combining 0.21 % Y and 0.15 % Ca on the steady-state creep rate of fine-grained annealed AZ80 at 50–100 MPa/125 °C. This research aimed to unravel the microscopic mechanism of Y and Ca on Al solute diffusion, precipitation, grain boundary movement, and dislocation movement. This work provides a theoretical basis for developing low-cost, creep-resistant wrought Mg alloys. In-situ electron back-scattered diffraction (EBSD) results demonstrated that discontinuous precipitation-induced grain boundary migration is the source of grain boundary instability in wrought Mg–Al alloys under medium-temperature creep conditions. The Ca alloying element is designed to segregate at the GB based on the segregation energy criterion and the GB migration activation energy. This reduces the diffusion of Al and the DP of the GB during the medium-temperature creep process, thereby stabilizing the medium-temperature GBs. The solute segregation to the GBs was investigated using HAADF-STEM, and the microalloying to increase the creep resistance of Mg–Al alloy at medium temperature is discussed.

2. Materials and methods

2.1. Materials preparation and processing

The AZ80 and (Y+Ca) microalloyed AZWX8000 were processed by resistance melting pure Mg (99.95 wt%), pure Al (99.9 wt%), pure Zn (99.9 wt%), Mg-30Y (wt%), and Mg-25Ca (wt%) master alloys. As Table 1 shows, the chemical

Table 1
The chemical compositions of the studied alloys (wt.%).

Alloys	Al	Zn	Y	Ca	Mg
AZ80	7.99	0.43	—	—	Bal.
AZWX8000	7.60	0.36	0.21	0.15	Bal.

Please cite this article as: L. Ren, Y. Zhao, J. Li et al., Inhibiting creep in fine-grained Mg–Al alloys through grain boundary stabilization, Journal of Magnesium and Alloys, https://doi.org/10.1016/j.jma.2024.04.033

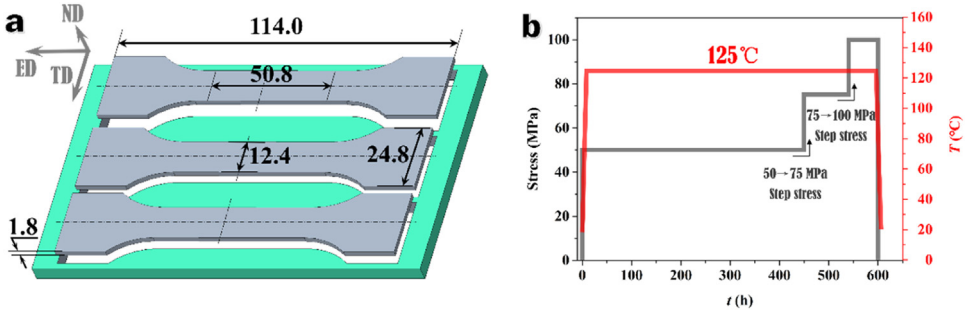

Fig. 1. Tensile-creep specimen preparation and schematic of the experimental creep-testing parameters. **(a)** The geometry of the tensile-creep specimens machined from the as-extruded sheets (ND, normal direction, TD, transverse direction, and ED, extrusion direction); all dimensions are provided in mm. **(b)** Schematic of the stress and specimen temperature, T, versus creep time, t, for the step-stress creep experiments.

compositions of the studied alloys were measured using an inductively coupled plasma mass spectrometer (ICP-MS). A covering flux and CO_2+2 vol.% SF_6 mixed gas protected the molten Mg from oxidation. The melt was held at 740 °C for 50–60 min and then poured into a mild steel die of 95 mm diameter. Homogenization annealing was conducted at 420 °C for 8 h, followed by air cooling. The billets were then machined into 88 mm diameter round bars. Before direct extrusion, the billets were preheated at 350 °C for 3–4 h. The extrusion container and die were preheated to 300 °C and 400 °C, respectively. Subsequently, the billets were extruded to 80 mm × 5 mm sheets with an extrusion ratio of approximately 16:1 at a 0.5–1.0 mm/s ram speed.

The tensile-creep specimens were cut along the extrusion direction (ED) of the extruded sheets using electrical discharge machining and had a 114.0 mm total length, 50.8 mm gage length and 12.4 mm × 1.8 mm cross-section (Fig. 1**(a)**). The tensile-creep samples were then ground using silicon carbide (SiC) papers through 400, 800, and 1200 grits (US standards) to reduce the surface processing damage, followed by ultrasonic bath cleaning with ethanol. To dissolve the β-$Mg_{17}Al_{12}$ precipitates and regulate the initial texture, 420 °C/4 h annealing was performed on the extruded AZ80 and AZWX8000 sheets in a sealed quartz glass tube.

2.2. Microstructural characterization

Metallographic samples were ground using SiC papers through 400, 800, and 1200 grits. The samples were then polished through 1.0 μm and 0.25 μm diamond pastes, and 0.04 μm colloidal silica solution was used for the final polishing. The samples were etched using a solution containing 60 ml ethanol, 20 ml water, 15 ml acetic acid, and 5 ml nitric acid. The microstructure of the alloys was observed using a ZEISS Axiolab 5 optical microscope and a TESCAN MIRA III FEG scanning electron microscope (SEM) equipped with an energy dispersive spectroscopy (EDS) system. An EDAX-TSL EBSD system was used to identify the grain size and texture. The step size was 0.2–0.4 μm, and at least 1000 grains were included in each EBSD map. Data postprocessing was performed using the EDAX OIM Analysis 7 software. The SEM accelerating voltage was 30 kV and the working distance was 16 mm. The precipitate characterization was performed by transmission electron microscopy (TEM, JOEL 2100F, 200 keV). Disks of 3 mm diameter were punched from the creep-tested specimens, ground to a thickness of 0.07 mm, and twin-jet electropolished in a solution of 4.4 g of lithium chloride, 9.3 g of magnesium perchlorate, 416.6 ml methanol, and 83.4 ml ethanol at −30∼−40 °C and 30 mA. The precipitate phases were also identified using a Bruker D8 ADVANCE X-ray diffraction (XRD) system with Cu $K_{\alpha 1}$ radiation (λ = 0.154 nm) at 2θ ranging between 30° and 80°.

2.3. Tensile and tensile creep testing

Tensile specimens with the same dimensions as the creep specimens (Fig. 1**(a)**) were electro-discharge machined along the extrusion direction (ED). Uniaxial tension tests were conducted at room temperature using a universal testing machine (MTS-CMT5105). A constant crosshead displacement rate (3.0 mm/min), corresponding to an initial strain rate of 10^{-3} s^{-1}, was maintained during the tests. Creep specimens were ground using SiC planar grinding papers through 400, 800, and 1200 grits. The specimens were then polished through 1.0 μm and 0.25 μm diamond pastes. Constant-load creep tests were performed using Applied Test Systems Incorporated (Butler, PA) lever arm creep machines. The test were performed using a 20:1 load ratio (a lever amplification of 20 times is used to apply a fixed load to the specimen), in air at 125 °C and applied stresses ranging between 50 and 100 MPa. The creep strain was continuously measured throughout the test using a linear variable differential transformer attached to the gage section. A three-zone split furnace and a current proportioning temperature controller maintained the test temperature within ±1 °C. The specimen temperature was measured using spot-welded chromel-alumel thermocouples on the surface of the gage section. All the creep tests lasted longer than 400 h. To investigate the influence of different stress levels on the steady-state creep rate, the creep tests were performed at step-stress levels of 50 MPa, 75 MPa, and 100 MPa [28,30]. Initially, the a creep test was performed under a load of 50 MPa for 400 h. Subsequently, the load was raised to

Please cite this article as: L. Ren, Y. Zhao, J. Li et al., Inhibiting creep in fine-grained Mg–Al alloys through grain boundary stabilization, Journal of Magnesium and Alloys, https://doi.org/10.1016/j.jma.2024.04.033

75 MPa for 40–70 h by increasing the weight, followed by an increase to 100 MPa for 5–20 h by further increasing the weight. All the applied creep stresses were kept below the yield strength. Fig. 1**(b)** illustrates the stress and temperature schedule during the tensile creep test. The continuous change in the cross-sectional area in the arc transition region produced a continuous tensile stress gradient when 100 MPa stress was applied to the gage section (see Fig. S1). Based on the arc transition region geometry parameters, the tensile stress along the tensile axis continuously decreased with the cross-section increase in the arc transition region. It would be useful to study the influence of stress gradient on the GB DP during intermediate-temperature creep in Mg–Al alloys.

3. Results

3.1. Microstructures and mechanical properties of the annealed AZ80 and AZWX8000

The annealed AZWX8000 exhibited a finer and more uniform microstructure than those for AZ80, which resulted in a narrower grain size distribution (Fig. 2**(c)**). The average grain size ($\bar{d}$) of the AZ80 was $\bar{d}$=37 ± 18 μm, which was approximately two times than that of the AZWX8000 ($\bar{d}$=20±8 μm), suggesting that the (Y+Ca) microalloying can effectively suppress the GB migration during annealing recrystallization [29]. In addition to the grain refinement, it should be noted that the (0001) basal texture intensity of the annealed AZ80 was similar to that of the annealed AZWX8000, which both eliminates the influence of texture variation or the creep comparison [30–34] and provides a constant texture basis for the follow-up single variable control studies of the impact of DP on the creep behavior of (Y+Ca) microalloyed Mg–Al wrought alloys. As revealed by the "Max" intensity value labeled in the (0001) pole figures in Fig. 2**(a and b)**, which represents the multiples of random distribution (MRD), the intensity of the (0001) basal texture was 15 MRD for both the annealed AZ80 and the annealed AZWX8000.

The (Y+Ca) microalloying has been shown to contribute to a fine-grained and textured annealed microstructure, which improves the mechanical properties of AZ80 sheets. The yield strength of the AZWX8000 was 160 MPa, which was about 50 MPa higher than that of the AZ80 (110 MPa), and the elongation-to-fracture of the AZWX8000 was 19.2 %, which was 5.1 % higher than that of the AZ80 (14.1 %). Thus, the (Y+Ca) microalloying increased the tensile strength and elongation-to-fracture for the annealed AZ80 sheets.

3.2. DP suppression enhanced creep resistance under similar initial texture

Fig. 3 shows that AZWX8000 exhibited greater creep resistance resulting from a lower DP than AZ80 under a similar basal texture intensity (15 MRD, see Fig. 2). The creep curves for AZ80 and AZWX8000 (Fig. 3**(a)**) show that AZWX8000 exhibited a lower creep strain, ε, than that of AZ80. For ex-

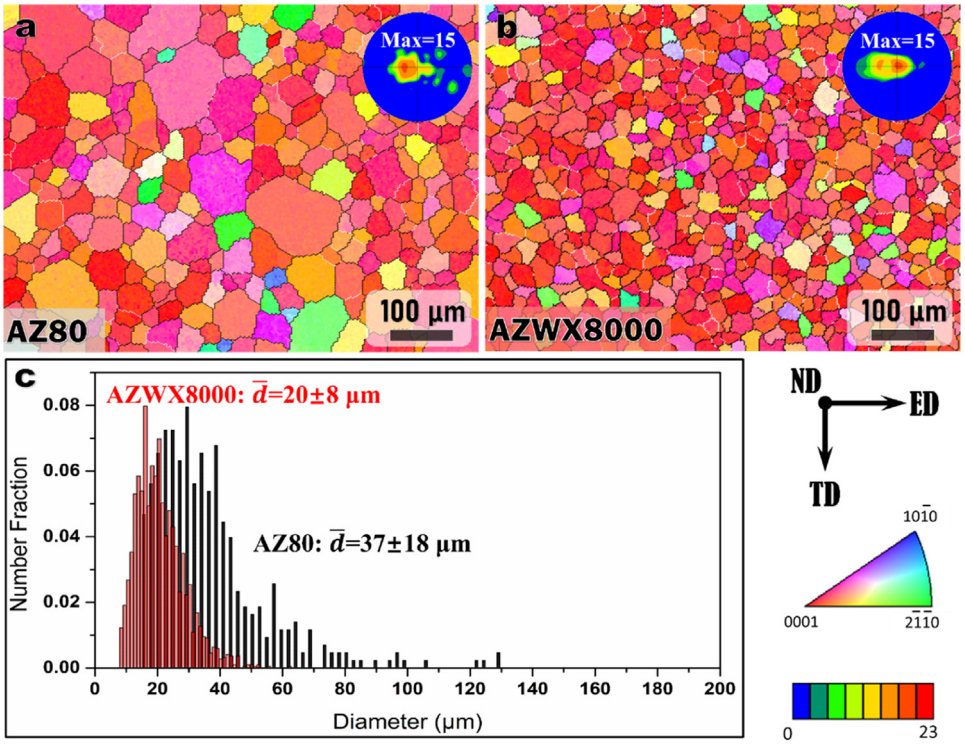

Fig. 2. AZWX8000 alloys exhibit a finer and more uniform grain structure than AZ80. EBSD crystal orientation maps and (0001) pole figures of **(a)** 420 °C/4 h annealed AZ80. **(b)** 420 °C/4 h annealed AZWX8000. **(c)** Grain size histograms of the studied alloys. The maximum intensity values are labeled in the (0001) pole figures in **(a and b)**, and the sample coordinate system, inverse pole figure color code, and texture intensity color scale are indicated at the bottom right.

Please cite this article as: L. Ren, Y. Zhao, J. Li et al., Inhibiting creep in fine-grained Mg–Al alloys through grain boundary stabilization, Journal of Magnesium and Alloys, https://doi.org/10.1016/j.jma.2024.04.033

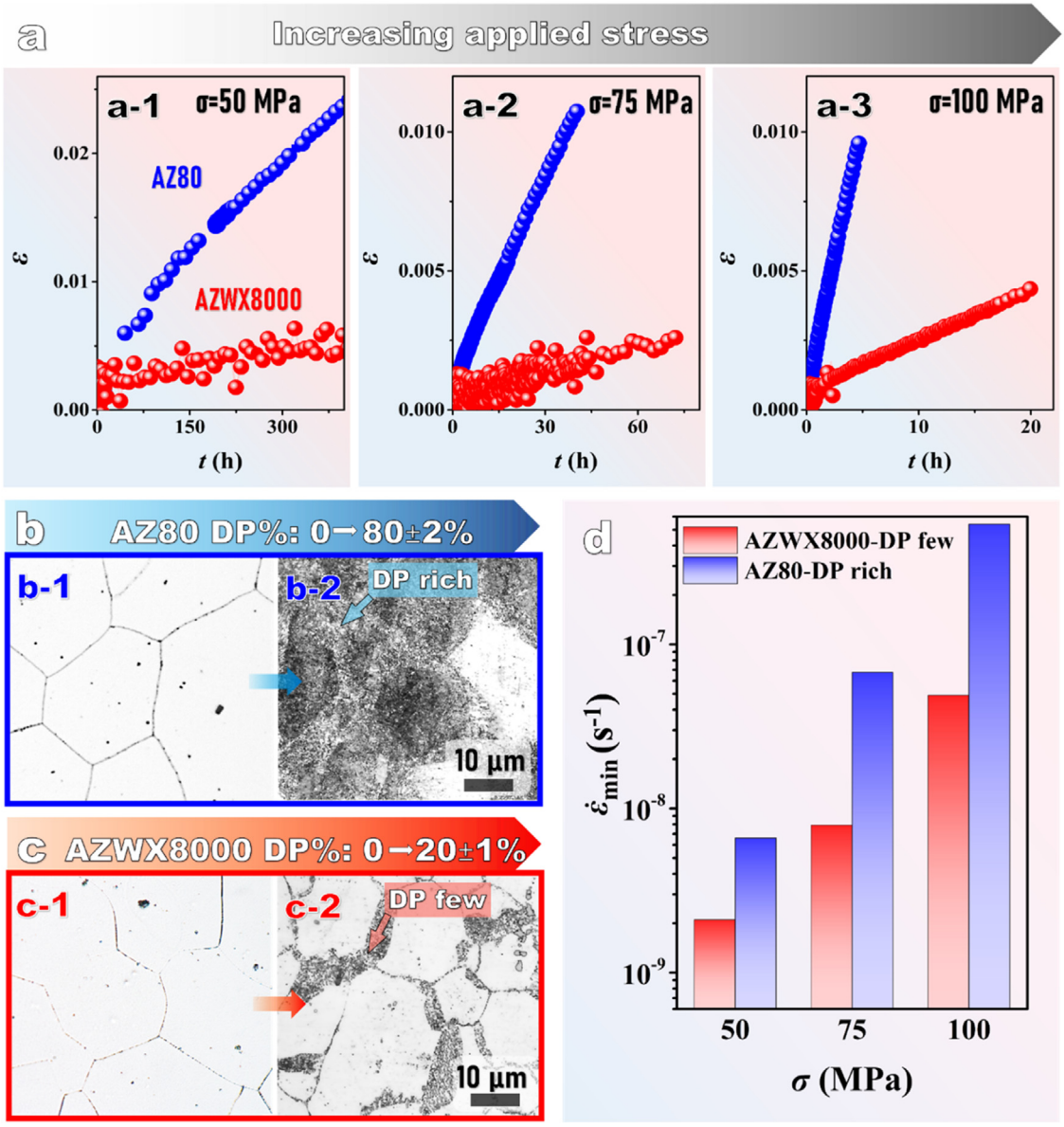

Fig. 3. AZWX8000 exhibits greater creep resistance resulting from a lower DP content than AZ80 under a similar basal texture intensity (15 MRD). **(a)** Creep strain, ε, variation with creep time, t, for AZWX8000 and AZ80 at 125 °C and stresses of **(a-1)** 50 MPa, **(a-2)** 75 MPa, and **(a-3)** 100 MPa. **(b)** and **(c)** optical photomicrographs before and after creep for AZ80 and AZWX8000, respectively. **(d)** Comparison of the minimum creep rate, $\dot{\varepsilon}_{min}$, for AZWX8000 and AZ80 at 125 °C in the applied stress range of 50–100 MPa.

ample, AZ80 exhibits 0.02 higher ε than AZWX8000 when creep tested at 50 MPa for 360 h (Fig. 3**(a-1)**). The ε increased rapidly when the stress increased from 50 MPa to 75 MPa or 100 MPa at 125 °C. For example, the ε of AZ80 reached 0.01 at σ=75 MPa and t = 40 h, which was two times higher than that of AZ80 tested at σ=50 MPa and t = 40 h (ε=0.005) (Fig. 3**(a-1, a-2)**).

Almost no DP was evident in either AZ80 or AZWX8000 before creep (see Fig. 3**(b-1)** and **(c-1)**), as most of the β-$Mg_{17}Al_{12}$ phases were dissolved into the α-Mg matrix during the annealing treatment. Both AZ80 and AZWX8000 presented β-$Mg_{17}Al_{12}$ XRD peaks for the post-creep specimens (Fig. 4), which indicates that β-$Mg_{17}Al_{12}$ precipitation in the form of DP occurred during the 125 °C creep (Fig. 3**(b-2, c-2)**). AZ80 exhibited a higher volume percent of DP content (80±2 vol.%) than AZWX8000 (20±1 vol.%) after the creep tests.

DP is sensitive to GB volume (or grain size) in Mg–Al alloys because GB diffusion dominates the DP growth at intermediate temperatures [35]. The fine-grained AZWX8000 should have exhibited more DP than the coarse-grained AZ80 because of the lower GB volume in the latter (Fig. 2**(b)**) [27]. However, the AZ80 exhibits four times more DP volume percent than the AZWX8000 after creep, which indicates that the (Y+Ca) microalloying effectively suppressed the DP growth during the intermediate-temperature creep. A higher volume percent of DP will contribute to a higher hardness value in Mg–Al alloys. The Vickers hardness in the gauge section for

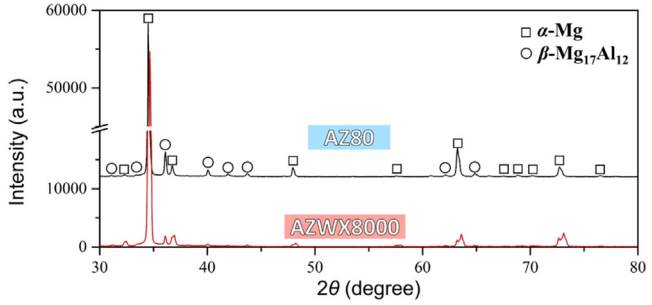

Fig. 4. X-ray diffraction pattern for AZ80 and AZWX8000 specimens after the creep tests.

the crept AZ80 was 101.3 ± 1.5, which was 27.1 higher than that for AZWX8000 (74.2 ± 0.5), and this is consistent with the difference in the DP volume percent between AZWX8000 and AZ80 described above.

Fig. 3**(d)** shows that the ε_{min} increased with increasing stress for the AZ80 and AZWX8000 at 125 °C/50–100 MPa, and the ε_{min} of AZWX8000 was lower than that for AZ80. For example, the (Y+Ca) microalloying resulted in a decrease in ε_{min} from 5.4 × 10^{-7} s^{-1} (AZ80) to 4.9 × 10^{-8} s^{-1} (AZWX8000) for creep conditions of 125 °C/100 MPa (Table 2). The (Y+Ca) microalloying resulted in an order of magnitude decrease in the minimum creep rate at 125 °C/50–100 MPa.

Table 2
The minimum creep rate, ε_{min}, for the studied alloys at 50 MPa, 75 MPa, and 100 MPa.

Alloys	Stress/MPa	$\varepsilon_{min}/\times 10^{-9}$
AZ80	50	6.6
	75	67.6
	100	540.0
AZWX8000	50	2.1
	75	7.9
	100	48.9

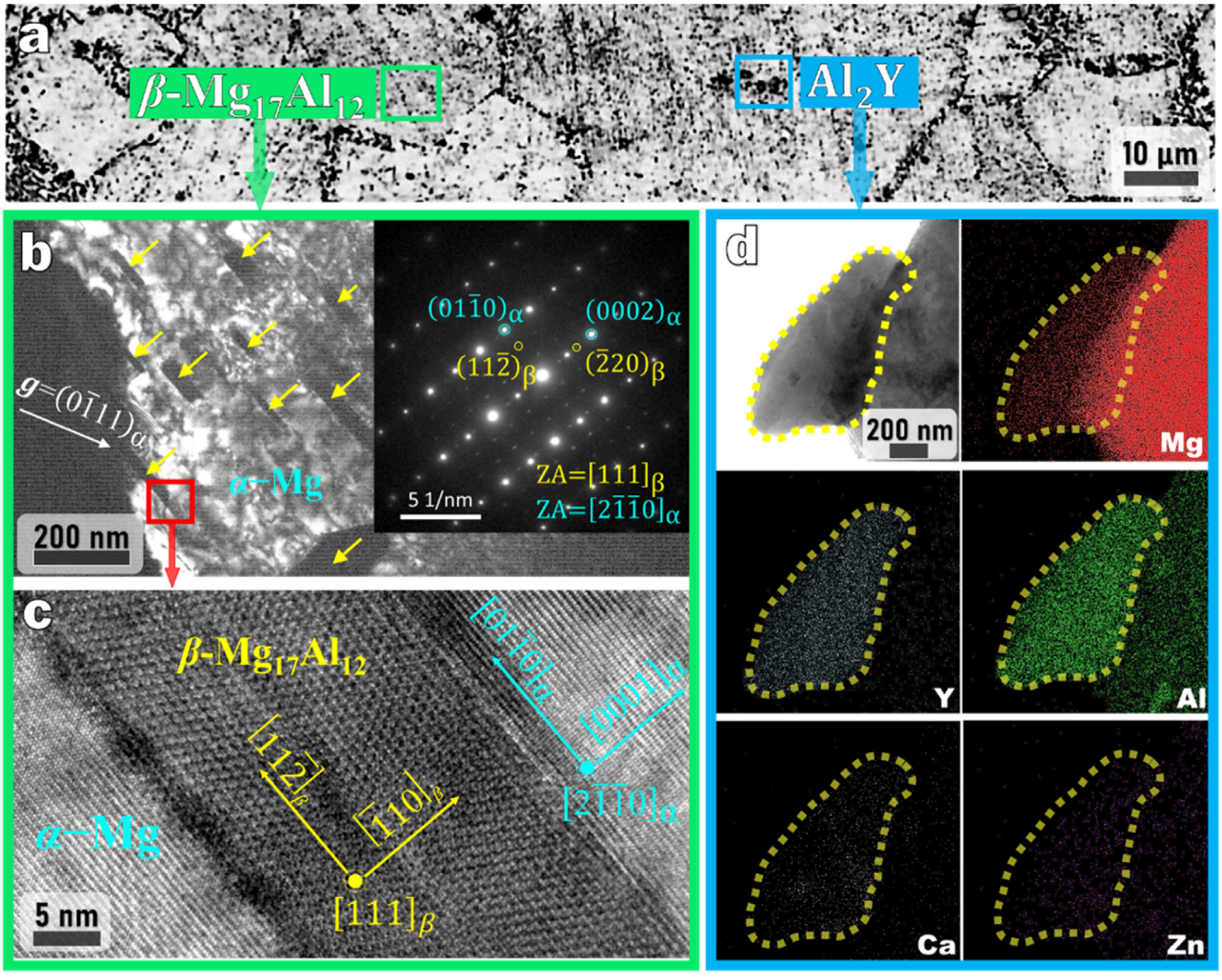

Fig. 5. (Y+Ca) microalloying enhanced intragranular precipitation in AZWX8000 during creep. **(a)** The post-creep optical photomicrograph of AZWX8000 shows the finer intragranular precipitation containing rod-like β-$Mg_{17}Al_{12}$ and Al_2Y particles. **(b)** Corresponding TEM bright field image of the green rectangular area in **(a),** revealing the fine intragranular rod-like β-$Mg_{17}Al_{12}$ precipitates (yellow arrows) formed on the basal plane. The electron diffraction patterns are labeled in **(b)**, and the electron beam is parallel to $<2\bar{1}\bar{1}0>_{\alpha}$. **(c)** The enlarged region of the red rectangular area in **(b)** shows a high-resolution TEM image of a β precipitate. **(d)** STEM bright field image of the Al_2Y particles and corresponding EDS maps for the alloying elements.

Please cite this article as: L. Ren, Y. Zhao, J. Li et al., Inhibiting creep in fine-grained Mg–Al alloys through grain boundary stabilization, Journal of Magnesium and Alloys, https://doi.org/10.1016/j.jma.2024.04.033

3.3. Enriching finer intragranular precipitation during creep

Finely-dispersed precipitates hinder dislocation motion and slow the minimum creep rate in dislocation-controlled creep [19]. For example, Gibson et al. [36] reported that the Mg_2Sn precipitate morphology and stability in Mg–Sn–Zn alloys were altered by 0.1 wt% Na microalloying, which led to an ε_{min} approximately three orders of magnitude lower than that for the ternary Mg–Sn–Zn alloy at 177 °C/60 MPa. Zeng et al. [37] tried this approach in ring-rolled AZ80-Ag using a pre-aging treatment, and they found that the continuous precipitate-dominated microstructure significantly enhanced the creep resistance at 120–175 °C/70–90 MPa. In this work, unlike the large-sized $\alpha+\beta$ lamellar precipitates that formed in the vicinity of the GBs during intermediate-temperature (100–200 °C) aging treatments in other Mg–Al alloys [21], the finely-dispersed intragranular precipitates, which were continuous, nanosized, and with high number density (Fig. 5), formed during the dynamic precipitation during creep of AZWX8000. Therefore, it is suggested that a microstructure with a high-volume fraction of the dynamically-formed intragranular nanoscale precipitates improves the creep resistance.

Two typical dynamic intragranular precipitates were present in the creep-deformed AZWX8000 sample, including the rod-like β-$Mg_{17}Al_{12}$ and Al_2Y particles, as shown in Fig. 5**(a)**. Fig. 5**(b, c)** shows that the corresponding TEM bright field image and the high-resolution TEM image of the intragranular β precipitates, which illustrated that the β precipitates formed on the (0001) basal plane and exhibited an orientation relationship between the β precipitates and the α-Mg matrix: $(0002)_\alpha \parallel (\bar{2}20)_\beta$, $[01\bar{1}0]_\alpha \parallel [11\bar{2}]_\beta$. These finely-dispersed nanosized β precipitates enhance the dislocation-hindering effect during creep [12,38]. The STEM bright field image of the Al_2Y particles and the corresponding EDS maps for the alloying elements are shown in Fig. 5**(d)**. Y microalloying brings Al_2Y particles into the AZWX8000, where the thermally-stable (melting point ~1490 °C [39]) and hard (elastic modulus~152 GPa [11,40]) intragranular particles contribute additional dislocation-hindering on the intermediate-temperature creep.

4. Discussions

4.1. In-situ observations of the discontinuous precipitation-induced grain boundary instability

The GB stability (sliding, migration) affects the creep properties of Mg alloys. GB migration was observed in situ using EBSD to verify the effect of DP on the GB stability of AZ80. The GB position changes were quantitatively com-

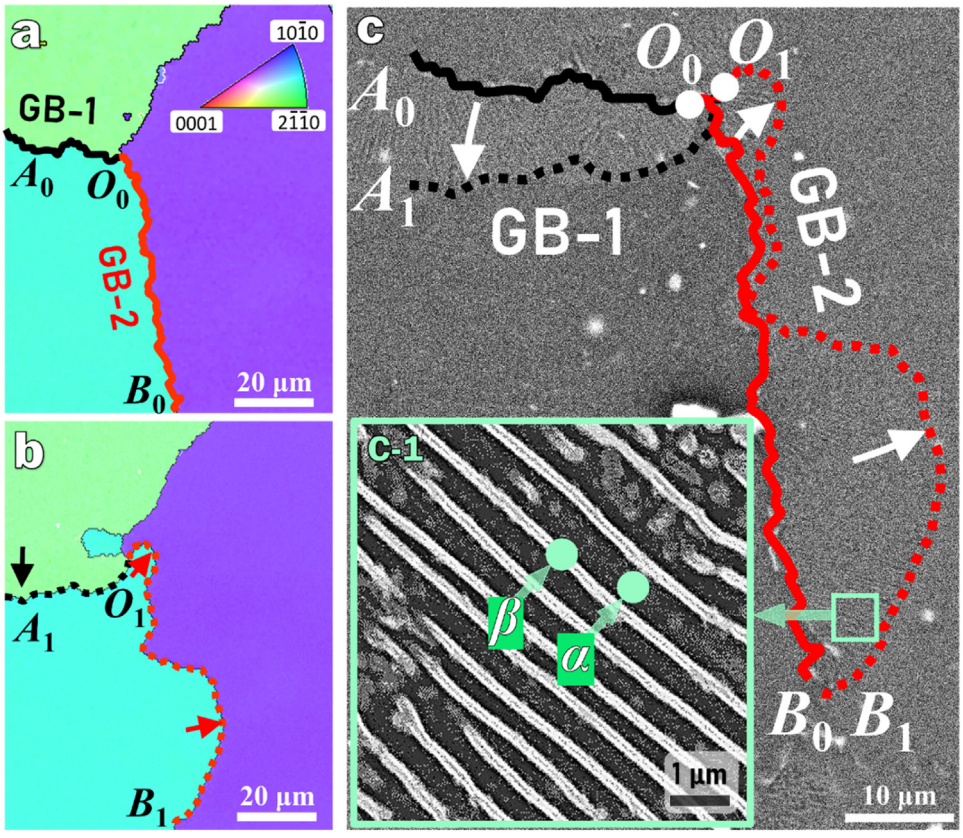

Fig. 6. In-situ observation of GB migration during DP growth. EBSD orientation map showing the annealed microstructure in **(a)** and after subsequent 170 °C/5 min aging in **(b)** for the AZ80. **(c)** In-situ representation of the trace line of GB motion in **(a and b)** on the backscattered electron image, and **(c-1)** shows the alternating plates of the α-Mg matrix and β-$Mg_{17}Al_{12}$ secondary phase behind a moving GB during DP growth. The inverse pole figure color code is indicated in **(a)**.

Please cite this article as: L. Ren, Y. Zhao, J. Li et al., Inhibiting creep in fine-grained Mg–Al alloys through grain boundary stabilization, Journal of Magnesium and Alloys, https://doi.org/10.1016/j.jma.2024.04.033

pared before and after aging at 170 °C/5 min. Fig. 6(a) shows that two α-Mg grain boundaries, GB-1 (O_0-A_0) and GB-2 (O_0-B_0), were tracked using EBSD orientation mapping. GB-1 migrated from O_0-A_0 to O_1-A_1, and GB-2 migrated from O_0-B_0 to O_1-B_1 (Fig. 6**(b)**). The in-situ trace lines of GB-1 and GB-2 were presented in the backscattered electron SEM image in Fig. 6**(c)**. A quantitative analysis of the GB positions indicated uniform GB motion during the DP growth. For example, the maximum GB migration rates ($V_{GB\ (max)}$) of GB-1 and GB-2 reached 2.5 μm/min and 4 μm/min, respectively, while the migration rates of the triangular GB and the GB-2 middle part were near 0 μm/min. In addition, there were alternating plates of the α-Mg matrix and β-$Mg_{17}Al_{12}$ secondary phase behind a moving GB during DP growth (Fig. 6**(c-1)**), and the average interlayer spacing between the α and β phases was approximately 620 nm.

DP growth is a prevalent creep microstructure evolution feature during intermediate-temperature creep in Mg–Al alloys [27]. According to Fig. 3**(b and c)**, AZ80 and AZWX8000 exhibit DP growth during creep at 125 °C/50–100 MPa. The in-situ experimental results illustrate that the GB instability originates from the DP growth during the creep at 125 °C/50–100 MPa. Therefore, suppressing DP growth during intermediate-temperature creep will enhance GB stability and improve creep resistance.

$$v_n = MF \tag{1}$$

$$M = M_0 exp(-Q/k_bT) \tag{2}$$

The fundamental kinetic equation for GB motion is expressed as Eq. (1) [41]. It shows that the boundary normal velocity (v_n) is linearly related to a driving force (F) through the GB mobility (M). Eq. (2) shows that the mobility of the thermally-activated GBs decreases with the increase of the activation energy, Q, which restricts the kinetic exchange rate of atoms between neighboring grains. Due to its largely negative GB segregation energy values [42], the Ca alloying element prefers to be located at the boundary having high activation energies, suggesting that the Ca solute can immobilize boundaries.

4.2. (Zn+Ca) co-segregation enhancing the grain boundary stability

The tension creep results of AZWX8000 in Fig. 3 indicate that the (Y+Ca) microalloying can suppress the DP

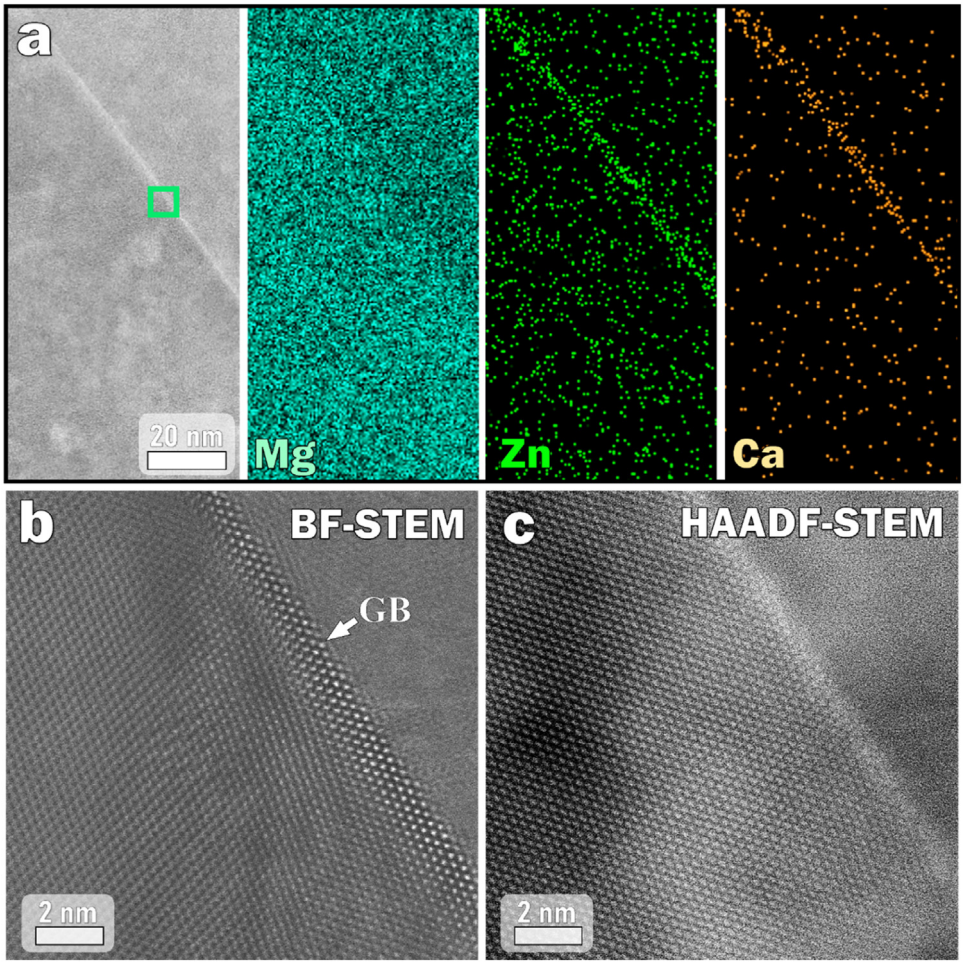

Fig. 7. Zn and Ca segregation at the grain boundary in AZWX8000. **(a–c)** The HAADF-STEM image and EDS map show Zn and Ca solute segregation to grain boundaries. (b) and **(c)** The enlarged region of the green rectangular area in **(a)** shows BF-STEM and HAADF-STEM images of the grain boundary.

Please cite this article as: L. Ren, Y. Zhao, J. Li et al., Inhibiting creep in fine-grained Mg–Al alloys through grain boundary stabilization, Journal of Magnesium and Alloys, https://doi.org/10.1016/j.jma.2024.04.033

growth by 75 % during creep at 125 °C/50–100 MPa, which enhances the intermediate-temperature creep resistance of wrought AZ80. An original microstructural analysis near the GBs of AZWX8000 alloys was performed to investigate the micro-mechanism for improving the creep resistance, see Fig. 7. A HAADF-STEM image and its corresponding EDS maps indicated that there is both Zn and Ca solute enrichment at GBs. The BF-STEM and HAADF-STEM images in Fig. 7**(b and c)** provided more atomic scale details (Fig. 7**(a)**). There was a high atomic number contrast feature at the GBs, consistent with the Zn+Ca enrichment features. This TEM analysis revealedd that Zn and Ca microalloying elements (<0.5 wt%) tended to co-segregate at the GB in the Mg-Al solid solutions.

Some minor microalloying elements inhibited the GB diffusion-related microstructural features [43]. Somekawa's [42] first-principles calculation results indicated that the Zn and Ca solutes exhibit higher GB segregation energy than Y microalloying solutes in Mg solid solutions, which means the Zn and Ca solutes existing at GBs are more stable than Y or Al solutes, consistent with the (Zn+Ca) co-segregation at GBs in AZWX8000 (Fig. 7). On the other hand, Mahjoub et al. [41] studied the correlation between the GB segregation energy and the GB motion activation energy for different alloying elements. Their results suggested that the energy barrier to the motion of the general GBs is not directly related to the preference of the solute to partition to the GB. In other words, GB segregation is a necessary and insufficient condition of GB mobility hindering. First-principles calculation results [41] reveal that the Ca and Zn segregation solutes exhibit higher activation energies than those for the Y solutes for the GB mobility of Mg alloys. As a result, the Zn and Ca microalloying solutes in AZWX8000 tend to segregate toward GBs and increase the activation energy for GB mobility, which can effectively suppress GB migration induced by GB diffusion. In summary, the (Zn+Ca) co-segregation reduces the GB diffusion, thereby inhibiting GB migration assisted by DP growth and enhancing the intermediate temperature creep resistance of AZWX8000.

4.3. Constitutive analysis for the creep mechanism in the wrought Mg–Al alloys

According to the phenomenological constitutive relationship provided in Eq. (3), the dominant creep mechanism can be speculated through constitutive parameters, which is especially suitable for pure metals and/or stable single-phase microstructures [1,2]. In comparison, the creep mechanism becomes complicated for multiphase polycrystalline microstructures, such as those for wrought Mg–Al alloys, because multiple mechanisms work together in a given creep process [51,52].

$$\varepsilon_{min}kT/DGb = A(\sigma/G)^n(b/d)^p \tag{3}$$

where, ε_{min} is the minimum creep rate (s^{-1}), k is the Boltzmann constant (1.38 × 10^{-23} J/K), T is the absolute temperature (K), D is the diffusion coefficient (m^2/s), b is the Poisson vector, A is a constant, σ is the loading stress (MPa), and d is the grain size. Generally, diffusion creep mechanisms (e.g., Nabarro-herring or Coble creep) dominate the elevated-temperature creep at low stress [1]. Dislocation creep mechanisms (e.g., Harper–Dorn creep or solute drag creep) are prevalent in the intermediate-temperature range (100–200 °C) at relatively high stress [2,4,53]. For example, when the stress exponent $n = 1$, the creep activation energy Q = 130–135 kJ/mol, and the grain size exponent $p = 2$, the dominant creep mechanism of the Mg solid solution is Nabarro-Herring diffusion creep. When the stress exponent n = 4–7, the creep

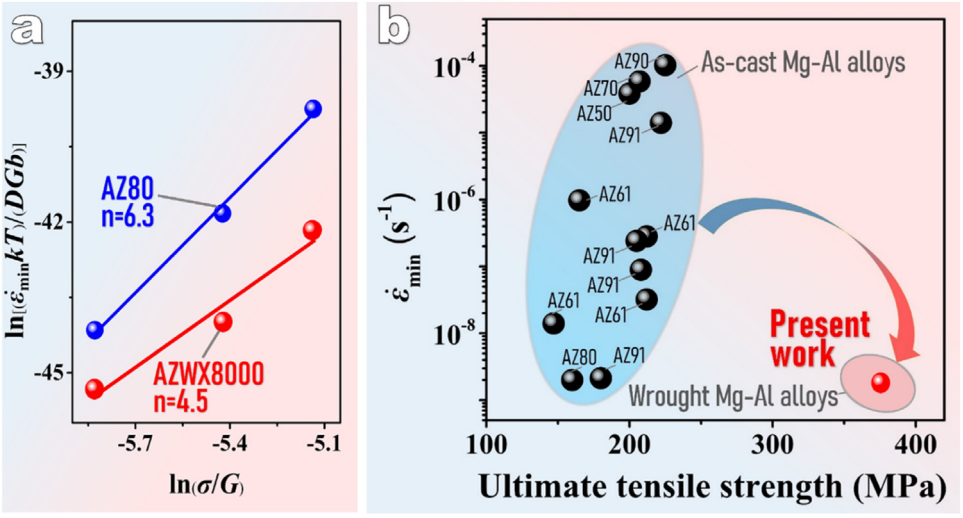

Fig. 8. Microalloying enhances the creep resistance of wrought Mg–Al alloys. **(a)** Constitutive analysis of the normalized minimum creep rate, $\dot{\varepsilon}_{min}$, versus the normalized stress in AZ80 and AZWX8000, where the corresponding stress exponent, n, is labeled in the plot. **(b)** In the present work, the creep-resistant wrought Mg–Al alloys exhibit a better balance of creep resistance and ultimate tensile strength than the Mg–Al alloy castings. It is noted that this is a fair comparison as the creep data of the cast Mg–Al alloys, including AZ50 [44], AZ61 [45–47], AZ70 [44], AZ80 [28], AZ90 [44], AZ91 [12,24,48–50], were collected at creep conditions of 125–150 °C/40–65 MPa. All tensile tests were conducted at room temperature and an initial strain rate of approximately 10^{-3} s^{-1}.

Please cite this article as: L. Ren, Y. Zhao, J. Li et al., Inhibiting creep in fine-grained Mg–Al alloys through grain boundary stabilization, Journal of Magnesium and Alloys, https://doi.org/10.1016/j.jma.2024.04.033

activation energy Q = 60–92 kJ/mol, and the grain size exponent p = 0, the primary creep mechanism of the Mg solid solution is a dislocation-controlled creep. Because the creep conditions investigated in this work involved medium-to-low temperatures and high-stress levels, the creep mechanism is expected to be dominated by dislocation creep, which is less sensitive to grain size than diffusion-dominated creep mechanisms. Therefore, the difference in initial grain size caused by microalloying is not expected to significantly impact the creep mechanism in this work.

As shown in Fig. 8**(a)**, the stress exponent of AZ80 and AZWX8000 was n = 6.3 and n = 4.5, respectively, under creep conditions of 125 °C/50–100 MPa. The constitutive analysis results suggest that the dislocation-controlled creep mechanism dominated the creep behavior in this work [18]. In addition, the GB segregation effect in AZWX8000 can not only effectively reduce the ε_{min} at the same stress level but also reduce the sensitivity of the steady-state creep rate to the loading stress (stress exponent) in the stress range of 50–100 MPa. This is expected to translate into improved creep resistance in the medium-to-high stress range.

The (Zn+Ca) GB co-segregation favored a finer and more uniform recrystallization structure after the hot extrusion processing and subsequent annealing treatment in AZWX8000 (Fig. 2**(b)**). The tensile strength, yield strength, and elongation-to-failure increased by 21 %, 41 %, and 30 %, respectively, between AZWX8000 and AZ80, resulting from the fine-grain strengthening. Fig. 8**(b)** shows that the microal-

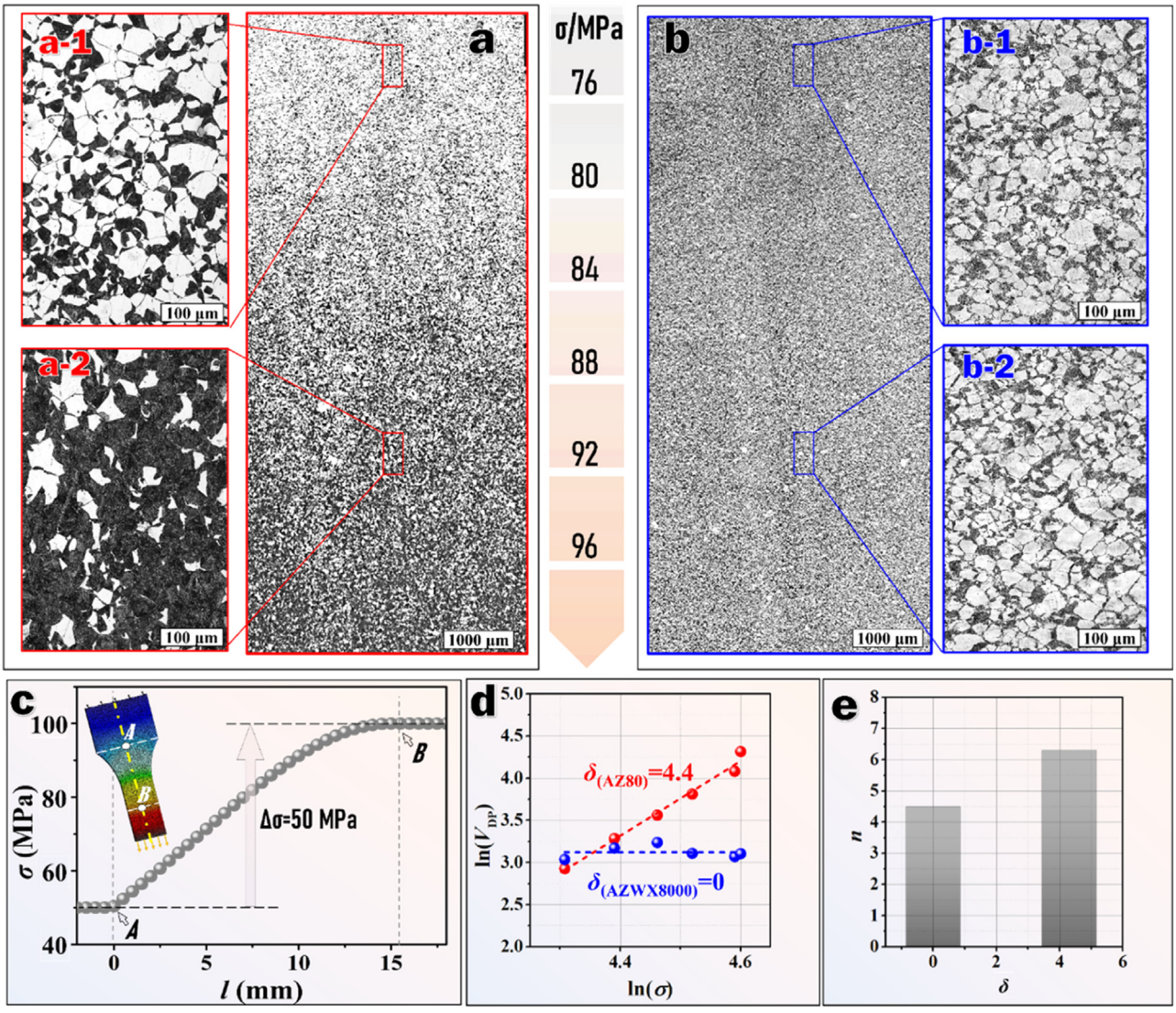

Fig. 9. Microalloying enhances the creep resistance stability in the 50–100 MPa creep stress range at 125 °C. The optical micrographs show the difference in the DP microstructure between **(a)** AZ80 and **(b)** AZWX8000 under the stress gradient of 75–100 MPa at 125 °C. **(a-1), (b-1)** is the enlarged optical micrograph of the DP containing microstructure for AZ80 and AZWX8000 at 75 MPa, respectively. **(a-2), (b-2)** is the enlarged optical micrograph of the DP containing microstructure for AZ80 and AZWX8000 at 92 MPa, respectively. **(c)** illustrates the stress gradient distribution at the transition region between the gauge and grip parts (***A-B***) in the creep test specimen. **(d)** DP volume fraction, $\ln(V_{DP})$, variation with creep stress, $\ln(\sigma)$, for AZWX8000 and AZ80 at 125 °C and AZWX8000 exhibits lower stress sensitivity to DP (δ=0) than AZ80 (δ=4.4), $\delta=\Delta(\ln(V_{DP}))/\Delta(\ln(\sigma))$. **(e)** Creep rate stress exponent, n, increases as the DP stress sensitivity, δ increases.

Please cite this article as: L. Ren, Y. Zhao, J. Li et al., Inhibiting creep in fine-grained Mg–Al alloys through grain boundary stabilization, Journal of Magnesium and Alloys, https://doi.org/10.1016/j.jma.2024.04.033

loyed AZWX8000 exhibited a lower ε_{min} under similar creep testing conditions and its tensile strength was almost double that of most as-cast Mg–Al alloys [12,24,28,44–50].

4.4. Microalloying enhances the creep resistance stability

Fig. 8**(a)** demonstrates that microalloying can decrease the stress exponent of AZ80 from $n = 6.3$ to $n = 4.5$, leading to improved creep resistance stability in the 50–100 MPa stress range at 125 °C. To investigate the microstructural causes of this reduced stress sensitivity, we analyzed the DP microstructure's sensitivity to stress in the *A-B* transition region under a 50–100 MPa stress gradient, as depicted in Fig. 9**(c)**. The microstructure of AZ80 and AZWX8000 under a stress gradient of 75–100 MPa/125 °C is compared in Fig. 9**(a)** and **(b)**. When subjected to increasing creep tensile stress (75→100 MPa), the DP volume percent in AZ80 increases from 19 % to 82 %, while in the transition region of AZWX8000, the volume percentage of DP remains stable at around 20 %. These changes align with the Vickers' hardness characteristics in both materials. Specifically, in AZ80, the Vickers hardness increases from 75 HV to 110 HV as the DP volume percent increases from 19 % to 82 %. In contrast, the Vickers hardness of AZWX8000 remains steady at approximately 75 HV in the transition region.

The microstructure of AZ80 and AZWX8000 after a creep test at 75 MPa and 92 MPa is depicted in Fig. 9**(a-1, a-2)** and **(b-1, b-2)**, respectively. The findings reveal that microalloying has a impact on reducing the creep stress sensitivity in dynamic DP growth. The sensitivity index 'δ' ($\delta = \Delta(\ln(V_{DP}))/\Delta(\ln(\sigma))$) measures the proportion of DP (V_{DP}) to creep stress (σ) in the stress range of 75–92 MPa. AZ80 exbibited a higher 'δ' value of $\delta_{(AZ80)}=4.4$ compared to AZWX8000 $\delta_{(AZWX8000)}=0$ (Fig. 9**(d)**). The analysis shows a positive correlation between the sensitivity exponent 'n' of steady creep rate to stress and the sensitivity index 'δ' of a proportion of DP to stress (Fig. 9**(e)**). The research findings above serve to confirm that the incorporation of microalloying agents has a significant impact on reducing the AZ80's creep rate stress sensitivity. The root cause of this effect lies in the microstructural changes induced by microalloying, which inhibit the stress sensitivity of dynamic DP during creep.

In summary, GB segregation is a crucial consideration in developing creep-resistant wrought Mg–Al alloys with attractive mechanical properties, and selecting appropriate microalloying combinations can provide desirable GB segregation. On the one hand, the (Zn+Ca) GB segregation in AZWX8000 inhibits Al solute GB diffusion, reduces DP-induced GB migration, and improves GB stability during intermediate-temperature creep. On the other hand, the GB diffusion inhibition resulting from GB segregation can promote intragranular Al solute diffusion. Higher Al solutes favor multiple Al-containing nano precipitates, including the rod-like β-$Mg_{17}Al_{12}$ and Al_2Y particles, which enhance the dislocation-hindering effect. The GB segregation stabilizes both the GB migration and intragranular dislocation motion during creep, thereby improving the intermediate-temperature creep resistance of wrought Mg–Al alloys.

5. Summary and conclusions

(1) Grain boundary instabilities can originate from discontinuous precipitation (DP)-induced grain boundary migration during the 125 °C/50–100 MPa creep in wrought Mg–Al alloys. 0.21Y+0.15Ca wt.% microalloying was shown to reduce the DP by 75 %, resulting in an order of magnitude enhancement in the tensile creep resistance of the studied Mg–Al sheets.
(2) The (Zn+Ca) grain boundary co-segregation inhibits GB diffusion and dynamic DP, promotes the enrichment of intragranular Al solute, favors multiple Al-containing nano precipitates (Al_2Y, $Mg_{17}Al_{12}$), and enhances the dislocation-hindering effect during creep.
(3) The DP-assisted dislocation-controlled creep mechanism dominates the intermediate-temperature creep behavior for wrought Mg–Al alloys. The Y+Ca microalloying decreases the creep stress exponent by 29 % (i.e., for AZ80, $n = 6.3$ and for AZWX8000, $n = 4.5$), and thereby results in improved creep resistance in the 50–100 MPa stress range at 125 °C.
(4) The (Zn+Ca) co-segregation favored a finer and more uniform recrystallization structure in the microalloyed AZWX8000 alloys, which exhibited a good balance between creep resistance, tensile strength, and elongation-to-failure.

Declaration of Competing Interest

The authors declare that they have no known competing financial interests or personal relationships that could have appeared to influence the work reported in this paper.

CRediT authorship contribution statement

Lingbao Ren: Writing – original draft, Project administration, Methodology, Investigation. **Yurong Zhao:** Writing – review & editing, Writing – original draft, Methodology, Investigation. **Jinjin Li:** Methodology, Investigation. **Fei Liu:** Methodology, Investigation. **Boyu Liu:** Writing – review & editing, Writing – original draft, Methodology, Investigation, Funding acquisition. **Ge Wu:** Writing – review & editing, Writing – original draft, Methodology, Investigation. **Carl J. Boehlert:** Writing – review & editing, Writing – original draft, Supervision, Project administration. **Zhiwei Shan:** Supervision.

Acknowledgments

The authors acknowledge the financial support from the National Natural Science Foundation of China (No: 52061040, No: 52371121, No: 52031011), China Postdoctoral Science Foundation (No: 2021M692512), and the 2020

open projects (No: KLATM202003) of Key Laboratory of Advanced Technologies of Materials, Ministry of Education China, Southwest Jiaotong University. The author thanks Siying Lu for the ICP-MS tests assistance and Yuanbin Qing, Xiaohua Cheng, and Shaochuan Zheng in the Center for Advancing Materials Performance from the Nanoscale for supporting SEM and TEM experiments.

Supplementary materials

Supplementary material associated with this article can be found, in the online version, at doi:10.1016/j.jma.2024.04.033.

References

[1] S.M. Zhu, M.A. Easton, T.B. Abbott, J.F. Nie, M.S. Dargusch, N. Hort, M.A. Gibson, Metall. Mater. Trans. A Phys. Metall. Mater. Sci. 46 (2015) 3543–3554.
[2] M. Pekguleryuz, M. Celikin, Int. Mater. Rev. 55 (2010) 197–217.
[3] Y. Yunqi, Z. Tingjie, D. Ju, Z. Lian, Rare Met. Mater. Eng. 33 (2004) 561–565.
[4] B.K. Atkinson, in: Creep of Crystals, 41, Cambridge University Press, 1985.
[5] R. Jing, Y. Jianshu, X. Faxiang, W. Jian, Study on heat of hydration on high strength concrete, J. Southeast Univ. Sci. Ed. 31 (2001) 53–56.
[6] Y. Lyu, A.R.M. Siddique, S.H. Majid, M. Biglarbegian, S.A. Gadsden, S. Mahmud, Electric vehicle battery thermal management system with thermoelectric cooling, Energy Rep. 5 (2019) 822–827.
[7] B.B. Zhang, Y.G. Tang, Q.S. Mei, X.Y. Li, K. Lu, Inhibiting creep in nanograined alloys with stable grain boundary networks, Science (80-.) 378 (2022) 659–663.
[8] T. Mineta, R. Suzumura, A. Konya, H. Sato, Mater. Today Commun. 34 (2023) 105502.
[9] S. Gavras, S.M. Zhu, J.F. Nie, M.A. Gibson, M.A. Easton, Mater. Sci. Eng. A 675 (2016) 65–75.
[10] I.P. Moreno, T.K. Nandy, J.W. Jones, J.E. Allison, T.M. Pollock, Scr. Mater. 48 (2003) 1029–1034.
[11] Z.W. Huang, Y.H. Zhao, H. Hou, P.D. Han, Phys. B Condens. Matter 407 (2012) 1075–1081.
[12] A. Srinivasan, J. Swaminathan, M.K. Gunjan, U.T.S. Pillai, B.C. Pai, Mater. Sci. Eng. A 527 (2010) 1395–1403.
[13] B. Backes, K. Durst, D. Amberger, M. Göken, Metall. Mater. Trans. A Phys. Metall. Mater. Sci. 40 (2009) 257–261.
[14] A.H. Eftekhar, S.M. Sadrossadat, M. Reihanian, Met. Mater. Int. 28 (2022) 1062–1074.
[15] C. Jun, Z. Qing, L.I. Quan-An, J. Alloys Compd. 686 (2016) 375–383.
[16] W. Yuan, S.K. Panigrahi, J.Q. Su, R.S. Mishra, Scr. Mater. 65 (2011) 994–997.
[17] J. Yan, Y. Sun, F. Xue, W. Tao, Jinshu Xuebao/Acta Metall. Sin. 44 (2008) 1354–1359.
[18] H. Somekawa, K. Hirai, H. Watanabe, Y. Takigawa, K. Higashi, Mater. Sci. Eng. A 407 (2005) 53–61.
[19] S. Ghosh, Contin. Mech. Thermodyn. 33 (2021) 2363–2374.
[20] I. Manna, S.K. Pabi, W. Gust, Int. Mater. Rev. 46 (2001) 53–91.
[21] D. Duly, M.C. Cheynet, Y. Brechet, Acta Metall. Mater. 42 (1994) 3855–3863.
[22] L. Zili, D. Wenjiang, Y. Guanyin, Z. Yanping, Mater. Mech. Eng. 25 (2001) 1–4.
[23] M. Montagnat, P. Duval, Earth Planet. Sci. Lett. 183 (2000) 179–186.
[24] M. Suresh, A. Srinivasan, K.R. Ravi, U.T.S. Pillai, B.C. Pai, Mater. Sci. Eng. A 525 (2009) 207–210.
[25] T. Homma, S. Nakawaki, S. Kamado, Scr. Mater. 63 (2010) 1173–1176.
[26] T. Homma, S. Nakawaki, K. Oh-Ishi, K. Hono, S. Kamado, Acta Mater. 59 (2011) 7662–7672.
[27] L.B. Ren, G.F. Quan, M.Y. Zhou, Y.Y. Guo, Z.Z. Jiang, Q. Tang, Mater. Sci. Eng. A 690 (2017) 195–207.
[28] L.B. Ren, C.J. Boehlert, G.F. Quan, Mater. Sci. Eng. A 801 (2021) 140397.
[29] L.B. Ren, M.Y. Zhou, C.J. Boehlert, G.F. Quan, J. Alloys Compd. 834 (2020), doi:10.1016/j.jallcom.2020.155077.
[30] J.A. del Valle, O.A. Ruano, Acta Mater. 55 (2007) 455–466.
[31] M. Heilmaier, F.E.H. Müller, G. Eisenmeier, B. Reppich, Scr. Mater. 39 (1998) 1365–1370.
[32] Z.Y. Xiao, Q.H. Huo, Y.X. Zhang, Z.R. Zhang, Z.H. Li, A. Hashimoto, X.Y. Yang, J. Alloys Compd. 823 (2020) 153754.
[33] J.H. Peng, Z. Zhang, Z. Liu, Y.Z. Li, P. Guo, W. Zhou, Y.C. Wu, Sci. Rep. 8 (2018) 4196.
[34] L.F. Wang, E. Mostaed, X.Q. Cao, G.S. Huang, A. Fabrizi, F. Bonollo, C.Z. Chi, M. Vedani, Mater. Des. 89 (2016) 1–8.
[35] D. Bradai, M. Kadi-Hanifi, P. Zięba, W.M. Kuschke, W. Gust, J. Mater. Sci. 34 (1999) 5331–5336.
[36] M.A. Gibson, X. Fang, C.J. Bettles, C.R. Hutchinson, Scr. Mater. 63 (2010) 899–902.
[37] G. Zeng, C.M. Liu, Y.C. Wan, Y.H. Gao, S.N. Jiang, Z.Y. Chen, Mater. Sci. Eng. A 734 (2018) 59–66.
[38] W. Blum, P. Zhang, B. Watzinger, B.V. Grossmann, H.G. Haldenwanger, Mater. Sci. Eng. A 319–321 (2001) 735–740.
[39] D. Qiu, M.X. Zhang, J. Alloys Compd. 586 (2014) 39–44.
[40] M. Rajagopalan, S. Praveen Kumar, R. Anuthama, Phys. B Condens. Matter 405 (2010) 1817–1820.
[41] R. Mahjoub, M. Ferry, N. Stanford, Comput. Mater. Sci. 210 (2022) 111042.
[42] H. Somekawa, A. Singh, R. Sahara, T. Inoue, Sci. Rep. 8 (2018) 1–10.
[43] E.D. Hondros, P.J. Henderson, Metall. Trans. A 14 (1983) 521–530.
[44] C.W. Lee, D.H. Song, K.Y. Nam, B.H. Choi, Y.H. Park, K.M. Cho, I.M. Park, Key Eng. Mater. 321–323 (2006) 1370–1373.
[45] C. Jun, Z. Qing, L.I. Quan-An, Int. J. Met. 12 (2018) 897–905.
[46] B. Kim, B. Kang, Y. Park, I. Park, Mater. Sci. Eng. A 528 (2011) 5747–5753.
[47] M.B. Yang, J. Shen, L. Bai, F.S. Pan, Int. J. Miner. Metall. Mater. 16 (2009) 89–95.
[48] G.Y. Yuan, Y.S. Sun, D.W. Jiang, Scr. Mater. 43 (2000) 1009–1013.
[49] B.H. Kim, S.W. Lee, Y.H. Park, I.M. Park, J. Alloys Compd. 493 (2010) 502–506.
[50] D.D. Zhang, D.P. Zhang, F.Q. Bu, X.X. Li, K. Guan, Q. Yang, S.H. Liu, X.J. Liu, J. Meng, Mater. Sci. Eng. A 693 (2017) 51–59.
[51] J.L. Yan, Y.S. Sun, F. Xue, W.J. Tao, Acta Metall. Sin. 44 (2008) 1354–1359.
[52] N. Kashefi, R. Mahmudi, Mater. Des. 39 (2012) 200–210.
[53] S.V. Raj, Mater. Sci. Eng. 96 (1987) 57–64.